9TH INTERNATIONAL SYMPOSIUM ON PARTICLE IMAGE VELOCIMETRY – PIV'11
Kobe, Japan, July 21-23, 2011

Volume Segmentation Tomographic Particle Image Velocimetry

I.B. Ziskin[1], R.J. Adrian[1], K. Prestridge[2]

[1]School for the Engineering of Matter, Transport, and Energy, Arizona State University,
Tempe, Arizona 85287-6106, USA
isaac.ziskin@asu.edu
rjadrian@asu.edu

[2]Los Alamos National Laboratory, Los Alamos NM 8754, USA

ABSTRACT

In tomographic PIV (TPIV) by volume segmentation images of particles in a volume are segmented into images on a set of planes. The planes of images can be analysed by standard mono- or stereo-PIV, and the volume of flow vectors can be recreated by assembling the planes of vectors. The interrogation process is similar to the HPIV analysis done in Barnhart, et al. [1], except that the planes of image data are extracted from two-dimensional camera images of the volume of particles instead of three-dimensional holographic images. Like the tomographic PIV method of Elsinga, et al. [2], planar segmentation requires at least two cameras and works best with three or four. Unlike the method of Elsinga, et al. [2], planar segmentation does not require reconstruction of individual particle images one pixel at a time, and it does not require an iterative process, so it operates much faster.

1. INTRODUCTION

Turbulence, by definition, is a fundamentally three-dimensional phenomenon; therefore, instantaneous three-dimensional three-component (3D3C) velocity measurements are one of the most important experimental contributions to the understanding of the turbulence problem. There have been several methods of expanding PIV to 3D3C including holography [1], photogrammetry [3], defocusing [4], and tomography [2]. Of these methods, Volume Segmentation is most similar to tomographic PIV. Both methods use the perspective images from multiple cameras to reconstruct the 3D information that is projected onto each camera's 2D image plane. This is done using mapping functions that are obtained during a pre-experiment calibration step as demonstrated by Soloff et al. [5]. These mapping functions describe how points in world coordinates are mapped to each individual camera's image coordinates. Tomographic PIV reconstructs the 3D measurements volume by back-projecting the gray-scale information from each image into the measurement volume, and iteratively correcting the 3D scene pixel-by-pixel until a satisfactory reconstruction is achieved [2]. Volume Segmentation differs from conventional tomographic PIV in that individual planes within the 3D measurement volume are reconstructed. This is done by operating on each entire image as opposed to each individual pixel and Volume Segmentation does not require multiple iterations to reach a satisfactory solution. In this way, Volume Segmentation is also similar the Multiplicative Line of Sight method reported by Atkinson and Soria [6] as well as a technique recently reported called Synthetic Aperture PIV [7] which uses a map-shift-average algorithm and a nine-camera system to reconstruct planes which they then assemble into a 3D reconstruction of the measurement volume. The major differences between these techniques are that Volume Segmentation uses interpolation and multiplication, and requires only three to four cameras. Also, 2D cross-correlation is used to obtain 2D2C velocity data and these are subsequently assembled into 3D3C velocity data through vector addition at corresponding interrogation volumes.

2. PLANAR SEGMENTATION

Volume Segmentation reconstructs individual planes within the 3D measurement volume in three computationally inexpensive steps: mapping, interpolation, and multiplication. The analysis procedure for Volume Segmentation is described below.

Before an experiment, mapping functions that describe how points in world coordinates (x,y,z) map to points in each camera's image coordinates (X_i,Y_i) are obtained following the procedure given by Soloff et al. [5]. Next the multiple camera PIV experiment is carried out as appropriate for the flow field being studied, see Adrian and Westerweel [8] for useful advice. The raw data from the experiment are single-exposed, double-frame, synchronized images of the particles within the 3D measurement volume. This raw data and the mapping functions unique to each camera obtained in the calibration step are all that are needed to begin analysis by Volume Segmentation. First an arbitrary Cartesian grid is chosen in world coordinates. The mapping functions are then used to map the points of a chosen plane in this grid to their corresponding points on each image. These points will map to fractional pixel locations, so the gray-scale-value information on each camera must be interpolated onto these subpixel locations. A bicubic spline is used because of its ability to preserve the high frequency information inherent in small particle images [9]. Now these subpixel gray-scale values correspond to real points in the fluid, and this information from each camera may be multiplied together and the product may be placed at the corresponding point in world coordinates. In this way, particles that belong in the chosen plane overlap in all of the images, causing them to be amplified by the multiplication process. Particles that do not belong to the chosen plane will most likely not overlap in all images causing them to be damped out because they are multiplied by the background of the image, which ideally has a gray-scale value of zero, but in most cases contains low-level noise.

This is repeated for planes both parallel and orthogonal to the optical axis of the camera system. The separation between the centers of the segmented planes may be chosen to be equal to the size of a pixel projected back into the volume. The effective thickness of these segmented planes is inherent in the

design of the experiment and is heavily dependent on the nominal size of a particle image projected back into the measurement volume.

Once the entire volume has been segmented, neighboring planes are summed together so that the desired image density is achieved. This is necessary because of the small thickness of the segmented planes as is shown in figure 6. These summed planes are then be analysed by conventional 2D cross-correlation to obtain 2D2C velocity data in each plane. These data are then combined to obtain 3D3C velocity data.

3. PARAMETRIC STUDY

The figures below show some trends of the Volume Segmentation technique from simulations of particles randomly placed in a 5x5x5mm^3 volume. Parameters that remained constant for all simulations are $f^{\#} = 16$, $M_0 = 0.3$, which made the nominal particle image diameter about 3 pixels, and all correlation coefficients shown were averaged over 201 planes. The data shown in Figures 1-3 was gathered using 4 simulated cameras at angles to the z-axis of -40°, -20°, 20°, and 40°. Figures 1-3 show that increasing the source density degrades the quality of the segmentation, just as it does for Tomographic PIV. Average correlation coefficients of 0.75 and 0.71 are obtained for particle concentrations of 8 and 12 particles/mm^3, respectively. The correlation coefficient is defined by equation (1).

$$Q = \frac{\sum I_{seg}(x,y,z)\sum I_{true}(x,y,z)}{\left(\sum {I_{seg}}^2(x,y,x)\sum {I_{true}}^2(x,y,z)\right)^{1/2}} \quad (1)$$

where I_{seg} and I_{true} are the segmented and true intensity planes, respectively. The source density N_s is defined by equation (2).

$$N_s = C\pi\left(\frac{d_\tau}{2M_0}\right)^2 l \quad (2)$$

where C is the mean particle concentration, d_τ is the diffraction limited particle image diameter, M_0 is the nominal magnification (calculated at the center of the measurement volume), and l is the effective depth of the line of sight through the measurement volume. The effective depth of the line of sight through the volume depends on the angle at which the camera observes the volume, so in this case the two inner cameras will have a slightly lower source density than the outer two cameras.

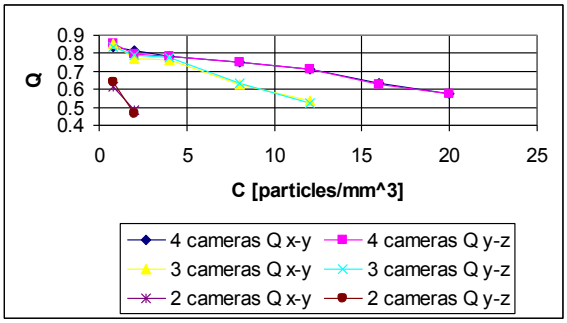

Figure 1. Correlation coefficient between segmented planes and the true planes they estimate versus mean particle concentration

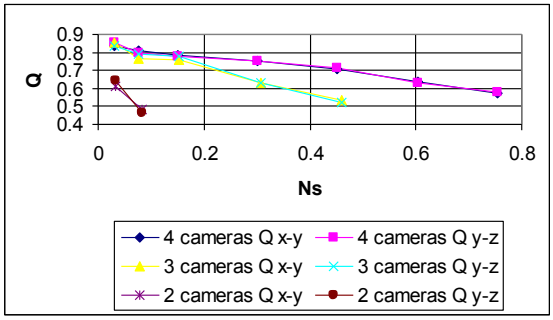

Figure 2. Correlation coefficient between segmented planes and the true planes they estimate versus source density

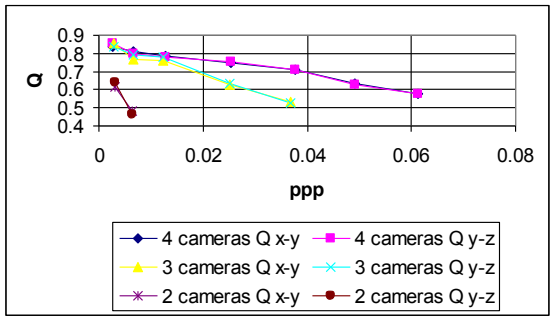

Figure 3. Correlation coefficient between segmented planes and the true planes they estimate versus particles per pixel

Figure 4 shows how the correlation coefficient changes with camera angle. Figure 5 shows how the effective thickness of the segmented planes changes with camera angle. The 4 cameras are always kept in a symmetric arrangement, and the inner cameras are kept at half the angle of the outer cameras. For example, when the angle in Figures 4 and 5 is 50° that means the cameras are arranged at the angles -50°, -25°, 25°, and 50° to the z-axis. All simulations for Figures 4-7 were performed with C = 8 particles/mm^3. The correlation coefficient shown in Figure 4 appears to level out between about 30° and 60°. It actually even appears to be slightly increasing with viewing angle beyond this region, but this effect would be mitigated by experimental conditions, e.g. refraction at the viewing window. Figure 5 also shows that optimum viewing arrangement has outer angles lying between 30° and 60°. The effective thickness of the segmented plane is found by cross-correlating one chosen segmented plane with all of the other segmented planes. The maximum correlation coefficient is found when the chosen plane is correlated with itself. The effective thickness is then found by measuring the full width at half maximum (FWHM) of the correlation coefficient curve. As can be seen in Figures 7 and 8, the thickness varies from one plane to another. The thickness of the x-y planes fluctuate about their mean value with an RMS of 12.19 microns and the thickness of the y-z planes fluctuate about their mean with an RMS of 9.10 microns.

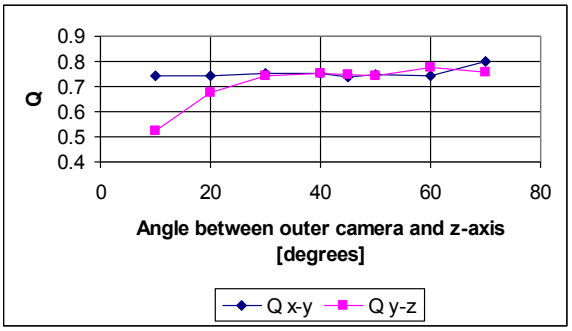

Figure 4. Correlation coefficient between segmented planes and the true planes they estimate versus the angle between outer camera and z-axis

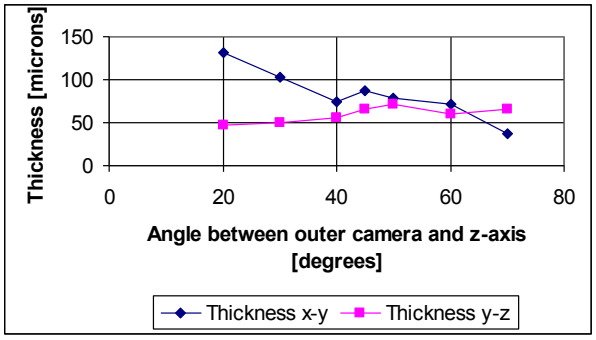

Figure 5. Effective thickness of segmented planes versus the angle between outer camera and z-axis

Figure 6. Correlation coefficient between segmented planes and the true planes they estimate versus calibration error in pixels

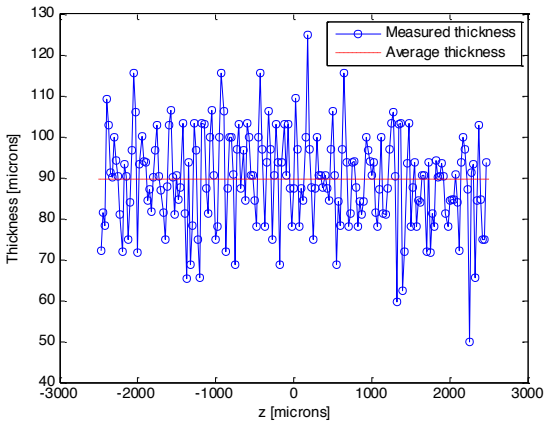

Figure 7. Effective thickness of segmented x-y planes with cameras oriented at -40°, -20°, 20°, and 40° from the z-axis and C = 12 particles/mm^3

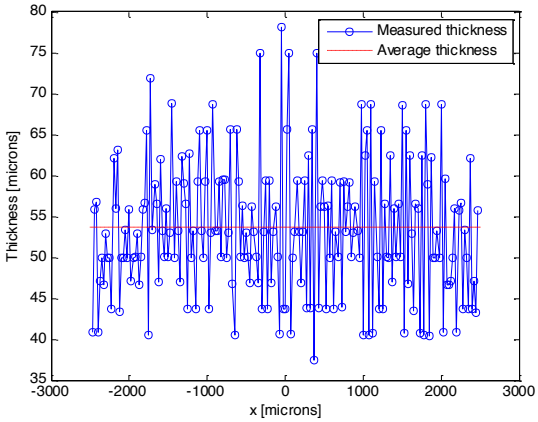

Figure 8. Effective thickness of segmented y-z planes with cameras oriented at -40°, -20°, 20°, and 40° from the z-axis and C = 12 particles/mm^3

4. CONCLUSIONS

ACKNOWLEDGEMENTS

This research was supported by Contract 79419-001-09, Los Alamos National Laboratory.

REFERENCES

[1] Barnhart, D.H., Adrian, R.J., & Papen, G.C. (1994) Phase-conjugate holographic system for high-resolution particle-image velocimetry. *Applied Optics,* **33(30)**, 7159-7170.

[2] Elsinga, G.E., Scarano, F., Wieneke, B. & van Oudheusden, B.W. (2006) Tomographic particle image velocimetry. *Experiments in Fluids*, **41**, 933-947.

[3] Maas H.G., Gruen A., & Papantoniou D. (1993) Particle tracking velocimetry in three-dimensional flows. *Experiments in Fluids*, **15**, 133–146.

[4] Pereira, F., Gharib, M., Dabiri, D., & Modarress, D. (2000) Defocusing digital particle image velocimetry: a 3-component 3-dimensional DPIV measurement technique. Application to bubbly flows. *Experiments in Fluids*, **29**, S78-84.

[5] Soloff S.M., Adrian R.J. & Liu Z.C.. (1997) Distortion compensation for generalized stereoscopic particle image velocimetry. *Measurement Science & Technology*, **8(12)**, 1441-1454.

[6] Atkinson, C. & Soria, J. (2009) An efficient simultaneous reconstruction technique for tomographic particle image velocimetry. *Experiments in Fluids*, **47**, 553-568

[7] Belden, J., Truscott, T.T., Axiak, M.C., & Techet, A.H. (2010) Three-dimensional synthetic aperture particle image velocimetry. *Measurement Science and Technology*, **21**, 1-21.

[8] Adrian, R.J. & Westerweel, J. (2010) *Particle Image Velocimetry*, Cambridge University Press.

[9] Astarita, T. & Cardone, G. (2005) Analysis of interpolation schemes for image deformation methods in PIV. *Experiments in Fluids*, **38**, 233-243.